



Magnetically recoverable nanoparticles for the simultaneous removal of Sb and As from water

M. Tzirini^a, E. Kaprara^b, T. Asimakidou^a, K. Kontogiannopoulos^c, E. Tzamos^c, I. Kellartzis^b, T. Samaras^a, Ll Balcells^d, M. Mitrakas^b, K. Simeonidis^{b,c,*}

^a Department of Physics, Aristotle University of Thessaloniki, 54124 Thessaloniki, Greece

^b Department of Chemical Engineering, Aristotle University of Thessaloniki, 54124 Thessaloniki, Greece

^c Ecoresources IKE, Giannitson-Santarosa Str. 15-17, 54627 Thessaloniki, Greece

^d Institut de Ciència de Materials de Barcelona, Campus Universitat Autònoma de Barcelona, A08193 Bellaterra, Spain

ARTICLE INFO

Keywords:

Arsenic
Antimony
Drinking water
Magnetic nanoparticles
Magnetic separation

ABSTRACT

This study examines the development of a nanocomposite consisting of iron oxy-hydroxides (FeOOH) embedded on magnetite (Fe₃O₄) nanocarriers, towards its application for the simultaneous uptake of As(V) and Sb(V) ionic forms at concentrations below drinking water regulation and its magnetically-assisted recovery at the end of the process. Considering Fe₃O₄ as the reductant, assisting the transformation of highly mobile Sb(V) to Sb(III), and the high affinity of FeOOH to adsorb both As(V) and Sb(III), adsorption experiments carried out at equilibrium pH 7 indicated that a FeOOH/Fe₃O₄ composition of 50%wt. is the optimum to establish a sufficient efficiency in the uptake of both pollutants. Particularly, the adsorption capacity for As(V) at residual concentration 10 µg/L is around 2.3 mg/g whereas around 0.4 mg/g of Sb(V) can be captured by the nanocomposite while keeping the residual concentration below 5 µg/L. Such efficiencies are preserved in the case of simultaneous adsorption of both pollutants without any appearance of cross-interference effects, at least for residual concentrations below 400 µg/L. The high magnetic response of Fe₃O₄ nanoparticles allows the application of the nanocomposite for water purification in an alternative setup, consisting of a contact stirring reactor and a magnetic separator constructed by permanent magnets. The dimensions and flowrates of the continuous-flow system were properly designed on the basis of theoretical calculations using the magnetization, adsorption efficiency and kinetics as input, to combine maximum purification and solid recovery. Suggestively, operation of the system using a natural water with pH 7 containing 50 µg/L As(V) and 10 µg/L Sb(V) showed successful decrease of residual concentrations below regulation limits for drinking water and 100% recovery of the solid when a nanocomposite's dose of 20 mg/L was added.

1. Introduction

Understanding the negative effect of specific water pollutants in consumers' life expectancy has pushed research efforts towards the improvement of water treatment strategies, quality control and relevant risk assessment (Geissen et al., 2015; Schwarzenbach et al., 2010; Wells et al., 2010). Among different types of pollutants, heavy metals represent the most important with geogenic origin. Their presence is commonly located in groundwaters due to the long-term contact with surrounding minerals (Chowdhury et al., 2016; Karavoltos et al., 2008), in the form of soluble oxy-ionic species which, when consumed at high concentrations, have been implicated with many chronic diseases, cancer development and vital organs failure (Hu et al., 2019; Kaltreider et al., 2001). Aqueous forms of antimony and arsenic are con-

sidered among the most harmful high priority heavy metal pollutants as implied by the extremely low regulation limits established by health organizations and local authorities for drinking water (Choong et al., 2007; Fei et al., 2017; Sarkar and Paul, 2016). Suggestively, the maximum contaminant level in European Union is 10 µg/L for arsenic and 5 µg/L for antimony (Council Directive 98/83/EC, 2000). Both elements belong to the metalloids group and therefore, they present some common characteristics regarding potential oxidation states. Depending on the accessibility of oxygen in the water reservoir, they can be found in the trivalent or the pentavalent state. However, the high-valent state, Sb(V) and As(V), dominates in the majority of the instances. Removing pentavalent species is usually the challenge for water treatment processes when facing high antimony or arsenic concentrations. Especially, in the pH range of natural water (6-8), the dom-

* Corresponding author at: Department of Chemical Engineering, Aristotle University of Thessaloniki, 54124 Thessaloniki, Greece.
E-mail address: ksime@physics.auth.gr (K. Simeonidis).

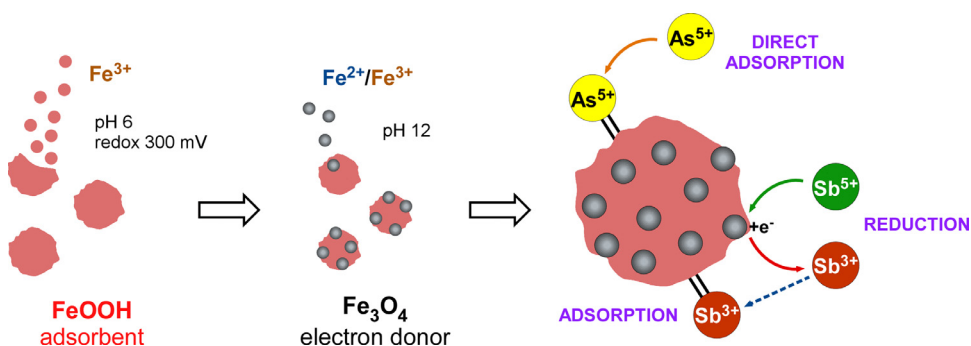


Fig. 1. Schematic representation of synthesis steps of $\text{Fe}_3\text{O}_4/\text{FeOOH}$ nanocomposites and occurring mechanisms during simultaneous $\text{As(V)}/\text{Sb(V)}$ adsorption.

inant speciation form of antimony is Sb(OH)_6^- while arsenic speciation is distributed between the H_2AsO_4^- and HAsO_4^{2-} oxy-anions (Scheinost et al., 2006; Tresintsi et al., 2012). The chemical similarity of antimony and arsenic often favors their co-occurrence as sulfide minerals (FeAsS , Sb_2S_3) implying to a high probability for simultaneous dissolution and co-existence in groundwater. Such cases have been reported in many sites across Greece and other European regions (Tresintsi et al., 2013; Ungureanu et al., 2015).

The presence of arsenic and antimony in water reservoirs may turn into a severe problem when these resources are used to supply drinking water, introducing the need to develop an extra treatment step for the capture of these pollutants before reaching the consumer. Following the high frequency of incidents where arsenic is the sole pollutant, development of relevant treatment methods has become the most discussed field of heavy metals removal from drinking water. Large-scale processes such as the coagulation with ferric salts and the adsorption on iron oxy-hydroxides (FeOOH) have been recognized as the best and viable practices (Lakshmanan et al., 2010; Mitrakas et al., 2009; Mohan and Pittman, 2007; Nicomel et al., 2015; Sankar et al., 2013). On the opposite side, due to the lower number of occurrences, not much attention has been devoted to the optimization of technologies for antimony uptake (Gannon and Wilson, 1986). Unfortunately, the implementation of adsorption systems, which appear very advantageous for point-of-use application with respect to its automation and feasibility, is inhibited by the high mobility of Sb(V) species and their weak affinity on any known adsorbent. Moreover, in the very possible scenario of arsenic co-existence, a significant competition for available adsorption sites has been reported (Tresintsi et al., 2013).

After that, the only way to face the problem of Sb(V) pollution in drinking water resources is to redesign known adsorbents or to match different phases in order to act in synergy through intermediate reaction mechanisms. Recently, composite nanomaterials consisting of amorphous oxy-hydroxides decorated with Fe_3O_4 nanoparticles have been introduced as a novel class of adsorbents able to capture Sb(V) oxy-ions after their intermediate reduction to Sb(III) species (Simeonidis et al., 2019). At the same time, the high affinity of FeOOH to As(V) (Tresintsi et al., 2012), and the magnetic response of Fe_3O_4 brings to these nanocomposites a high perspective to operate as efficient arsenic adsorbents on a water treatment scheme different than conventional fixed beds (Simeonidis et al., 2011).

This work investigates the possibility to develop an efficient and viable water treatment technology based on the low-cost production of $\text{Fe}_3\text{O}_4/\text{FeOOH}$ nanocomposites and apply them in a scalable contact reactor to purify antimony/arsenic polluted water. To this end, adsorbents with various phase ratios were synthesized into a continuous-flow reactor and then, tested in batch adsorption experiments to define the optimum adsorbent composition that delivers maximum uptake capacity for simultaneous presence of antimony and arsenic. Evaluation was performed under realistic conditions of water treatment including pollutants concentration range, pH values and eligible residual concentrations complying to the regulation limits. Taking advantage of the magnetic properties of embedded Fe_3O_4 nanoparticles, a water treatment

unit which combines sufficient adsorption period and complete adsorbent recovery was designed using arithmetic modeling of the magnetic separation stage.

2. Materials and methods

2.1. Synthesis

The synthesis of $\text{Fe}_3\text{O}_4/\text{FeOOH}$ nanocomposites was conducted in a two-stage continuous-flow stirring reactor (1 L each compartment) by the sequential precipitation of iron salts under different acidity and oxidative conditions (see Fig. S1 in Supporting information). In particular, the preparation of the iron oxy-hydroxide (FeOOH) was carried out in the first reactor by the precipitation of a $\text{FeSO}_4 \cdot 7\text{H}_2\text{O}$ solution (4.8 g/L) which is continuously pumped with a flowrate 0.5 L/h. The pH was adjusted and maintained at 6 throughout the operation by the addition of a 5%wt. NaOH solution whereas redox potential was increased and kept to around 300 mV by the addition of a 5% wt. H_2O_2 solution (Fig. 1). The FeOOH suspension was fed to the second tank, where the coprecipitation of $\text{FeSO}_4 \cdot 7\text{H}_2\text{O}$ and $\text{Fe}_2(\text{SO}_4)_3 \cdot x\text{H}_2\text{O}$ (20%wt. Fe basis) took place to produce Fe_3O_4 . A solution with a mixture of both reagents (2 g/L and 3.6 g/L, respectively) was introduced in this stage with a flowrate determined by the targeted Fe_3O_4 -to- FeOOH ratio in the product. For instance, to obtain a nanocomposite with Fe_3O_4 percentage around 50%wt., the flowrate was adjusted to 0.5 L/h. The pH was controlled to the value of 12 and the redox potential was decreased to around -180 mV as a result of the intense alkaline conditions but also by the addition of a 1%wt. hydrazine solution. The final product was collected from the outflow, washed with distilled water and centrifuged several times, dried at 40 °C, ground and sieved to below 63 μm . In order to ensure that all quantity of FeOOH will be totally loaded on the magnetic phase, the collected adsorbent was re-dispersed in water and then magnetically recovered by a permanent NdFeB magnet separating possible non-associated FeOOH grains.

2.2. Characterization

The identification of the crystal phases of the synthesized nanocomposites was performed through powder X-ray diffractometry (XRD) using a water-cooled Rigaku Ultima+ instrument with $\text{CuK}\alpha$ radiation, a step size of 0.05° and a step time of 2 s, operating at 40 kV and 30 mA. Diffraction diagrams were compared to the Powder Diffraction Files (PDF) database (Joint Center for Powder Diffraction Studies, 2004). The morphology of studied materials was examined by field-emission scanning electron microscope (FE-SEM) Quanta 200 ESEM FEG FEI with a field-emission gun operating at 30 kV and equipped with energy dispersive X-ray analysis (EDS) of EDAX. Quasi-static magnetic properties of the samples have been measured using a superconducting quantum interference device (SQUID) Quantum Design MPMS XL-7T magnetometer.

The specific surface area of samples was estimated by nitrogen gas adsorption at liquid N_2 (temperature 77 K) in a micropore surface area

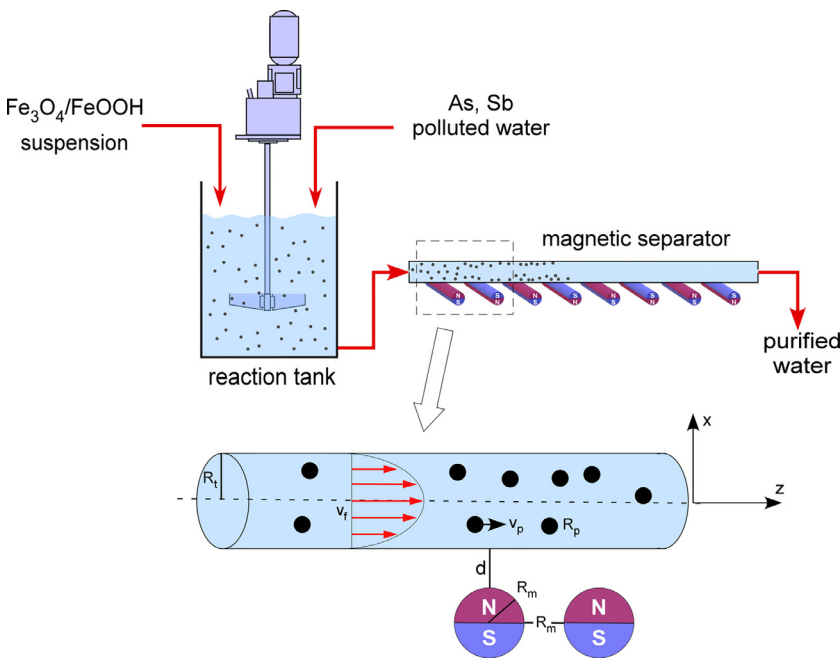


Fig. 2. Water treatment unit for As/Sb removal and modelling parameters of the nanocomposite’s magnetic recovery.

analyzer according to the Brunauer-Emmett-Teller (BET) model. Total iron content was measured after dissolution of weighted powders in HCl, by flame atomic absorption spectrophotometry using a Perkin Elmer PinAAcle 500 system. Finally, the reducing potential of nanocomposites expressed by the percentage of Fe²⁺ was determined by acid digestion of the solid followed by titration using KMnO₄ solution. A 50 mg sample was dissolved under heat in 20 mL 7 M H₂SO₄ and titrated with 0.05 M KMnO₄. The end point of the titration was defined by the presence of a persistent weak pink color, indicating that the MnO₄⁻ ions were no longer being reduced.

2.3. As/Sb adsorption

The efficiency of the adsorbents to capture the pentavalent forms of arsenic and antimony, separately and in their co-existence was evaluated by batch adsorption experiments plotting the corresponding isotherms at the low residual concentration regime (<500 µg/L). For each experiment, a quantity of 0.1 g/L from the nanocomposite was dispersed in 200 mL of As(V)- or Sb(V)- or As(V)/Sb(V)-containing test water (50-3000 µg/L) into a 300 mL conical flask and shaken for a sufficient period of time (24 h). The pH was adjusted to the value of 7 by the addition of drops of NaOH or HNO₃ during the first 2 h. At the end, the solid was discarded by filtering through a 0.45 µm membrane filter. The residual concentration of As and Sb was determined by a graphite-furnace atomic absorption spectrometer Perkin-Elmer AAnalyst 800. Corresponding kinetic experiments were conducted by mixing a specific quantity of the adsorbent with test solutions and sampling the pollutant’s residual concentration at proper time intervals.

Test solutions spiked with As(V), Sb(V) or a mixture of As(V) and Sb(V) were diluted in natural-like water (according to the National Sanitation Foundation (NSF) standard) in order to investigate the collective effect of common interfering ions in comparison to the distilled water. For the preparation of 10 L, 2.520 g NaHCO₃, 1.470 g CaCl₂•2H₂O, 1.283 g MgSO₄•7H₂O, 0.706 g NaSiO₃•5H₂O, 0.1214 g NaNO₃, 0.0221 g NaF and 0.0018 g NaH₂PO₄•H₂O were dissolved in distilled water.

2.4. Magnetic recovery

A major advantage of magnetic nanomaterials implementation in drinking water treatment is their magnetic response which enables different approaches of application compared to the typical filtration bed.

Here, the possibility of introducing the Fe₃O₄/FeOOH nanocomposite was evaluated according to observed uptake capacity and the magnetic properties in a continuous-flow system (Fig. 2), consisting of a contact tank where the nanomaterial is dispersed in polluted water and a cylindrical separation tube where particles are captured and recovered by the magnetic field defined by permanent magnets arranged along one side of the tube (Sharma et al., 2015). For the design of such magnetic separator, the optimum arrangement of eight commercial NdFeB magnets with cylindrical shape was studied by developing a two-dimensional theoretical model for dispersion flow which considers the balance of dominant magnetic F_m , fluidic forces F_f and buoyancy F_b (Furlani and Furlani, 2007):

$$\vec{F}_m + \vec{F}_f + \vec{F}_b = \vec{0} \tag{1}$$

Assuming non-interacting nanoparticles and an equivalent point dipole in the center of each carrier, the magnetic force is the sum of forces on the embedded magnetic particles analyzed as:

$$\vec{F}_m = \mu_0 V_{mp} \frac{3\chi_p}{\chi_p + 3} (\vec{H} \nabla) \vec{H} \tag{2}$$

which, for a magnetic susceptibility $\chi_p \gg 1$ it is simplified as:

$$\vec{F}_m = 3\mu_0 V_{mp} (\vec{H} \nabla) \vec{H} \tag{3}$$

and considering the average particles “magnetic” volume $V_{mp} = \frac{4}{3}\pi R_{mp}^3$, leads to:

$$F_{mx} = 4\pi\mu_0 R_{mp}^3 \left(H_x \frac{\partial H_x}{\partial x} + H_z \frac{\partial H_x}{\partial z} \right) \tag{4}$$

$$F_{mz} = 4\pi\mu_0 R_{mp}^3 \left(H_x \frac{\partial H_z}{\partial x} + H_z \frac{\partial H_z}{\partial z} \right) \tag{5}$$

with R_{mp} the particles’ “magnetic” radius, i.e. the radius corresponding to their magnetic phase, μ_0 the permeability of air, H the applied magnetic field intensity. The magnetic field components for an infinite cylindrical magnet, magnetized perpendicularly to its axis, given at reference system ($x'-z'$) defined at its center (Furlani and Ng, 2006), are:

$$H_{x'} = \frac{M_s R_m^2}{2} \frac{x'^2 - z'^2}{(x'^2 + z'^2)^2} \tag{6}$$

$$H_{z'} = \frac{M_s R_m^2}{2} \frac{2x'z'}{(x'^2 + z'^2)^2} \tag{7}$$

where M_s and R_m are the magnetization and radius of the magnet, respectively.

Fluidic forces are described by Stokes' approximation for sphere in laminar flow:

$$\vec{F}_f = -6\pi\eta R_p(\vec{v}_p - \vec{v}_f) \quad (8)$$

with components:

$$F_{fx} = -6\pi\eta R_p v_{px} \quad (9)$$

$$F_{fz} = -6\pi\eta R_p \left\{ v_{pz} - 2\bar{v}_f \left[1 - \left(\frac{x}{R_t} \right)^2 \right] \right\} \quad (10)$$

where η is the fluid's viscosity, R_p the particles' radius, v_p is the particle flow velocity and $v_f = \frac{Q}{\pi R_t^2}$ is the average flow velocity, while Q stands for volume flow rate. The buoyancy term is expressed by the equation:

$$\vec{F}_b = -V_p(\rho_p - \rho_f)\vec{g} \quad (11)$$

Since the buoyancy term is vertical, its only component is given by:

$$F_{bx} = -\frac{4}{3}\pi R_p^3(\rho_p - \rho_f)g \quad (12)$$

with ρ_p the density of particles, ρ_f the density of the fluid and g the gravitational acceleration. The recovery efficiency for each tested setup was predicted by computing the tracks of several nanoparticles after solving the motion equations with a 4th order Runge-Kutta (RK4) scheme in Matlab. Acting magnetophoretic force as well as the equations of motion were obtained by Mathematica (Supporting information). As design parameters, the tube radius R_t , the magnets radius R_m which was equal to the distance between magnets, the relative position d and the polarity configuration N/S, were used as explained in Fig. 2. Optimum parameters extracted by the theoretical simulation were used to construct and operate the corresponding scalable laboratory setup and validate the accuracy of the predictions.

3. Results and discussion

3.1. Adsorbents' characterization

XRD diagrams of the synthesized $\text{Fe}_3\text{O}_4/\text{FeOOH}$ nanocomposites are shown in Fig. 3. For all compositions, an inverse spinel structure of iron oxide (possibly Fe_3O_4) is clearly identified while the increase of an amorphous background contribution at lower magnetic phase percentages signifies the presence of FeOOH.

The formed phases are homogeneously distributed in the volume of the nanocomposite as better observed in FE-SEM images of the 50% sample (Fig. 4a). The nanocomposite adsorbent has a sponge-like morphology suggesting the deposition and dispersion of iron oxide nanoparticles during the second reaction step into the previously precipitated amorphous oxy-hydroxide structure. In addition, obtained nanocomposites show good mechanical stability, indicating that no dissociation of the constituting phases is expected to occur. Such technological characteristic is very critical when referring to nanomaterials application for water treatment (Tresintsi et al., 2012). Iron oxy-hydroxide's matrix seems to define the obtained hydrodynamic diameter of the adsorbent, which is estimated to be around 500 nm without significant variation between the samples (Fig. 4b). This value fits well to the average dimension of the aggregates appearing in electron microscopy images although the expected diameters of Fe_3O_4 nanoparticles when synthesized separately with the same procedure is only around 40 nm (Simeonidis et al., 2015). The described nanostructure is reflected in the nitrogen adsorption isotherms where a smooth, non-stepwise curve, probably associated with energetic heterogeneity in the adsorbent-adsorbate interaction, is found (Fig. 4c). In addition, the presence of hysteresis during desorption

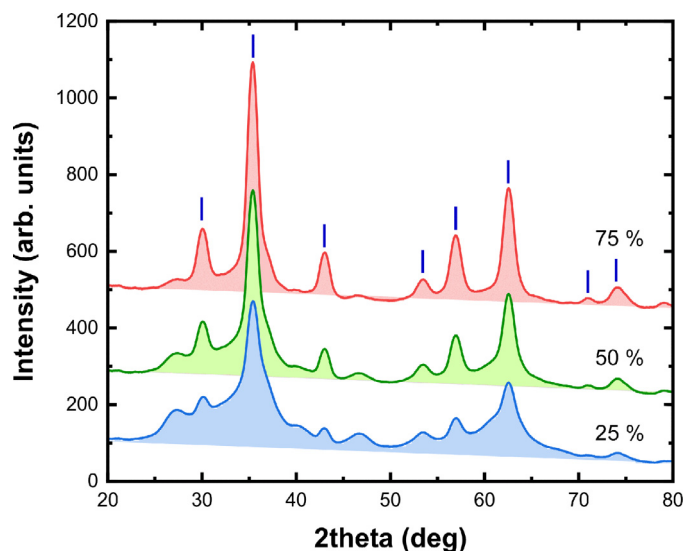


Fig. 3. XRD diagrams of $\text{Fe}_3\text{O}_4/\text{FeOOH}$ nanocomposites for various magnetic phase percentages. Vertical lines indicate the expected diffraction angles for magnetite (PDF#88-0315).

indicates a low percentage of micropores attributed to the formation of intraparticle porosity in the building units of the FeOOH. The specific surface area of samples was estimated in the range 105-120 m^2/g with the lower values corresponding to the Fe_3O_4 -rich samples.

The iron content of studied nanocomposites was measured by chemical analysis indicating a percentage of 48.3%wt. in the sample with 25% Fe_3O_4 that reaches 50.9%wt. in the sample with 75% Fe_3O_4 . This information does not provide important findings concerning their composition, since iron is the only existing metal in both participating phases. However, determination of the Fe^{2+} species corresponds to the presence of Fe_3O_4 , while it is also a good indicator of the reducing potential of each adsorbent. Particularly, the Fe^{2+} percentage per mass of nanocomposite was found to be 5, 9.5 and 11%wt. respectively for the samples prepared with 25, 50 and 75% Fe_3O_4 . Magnetic characterization was used as another way to estimate samples composition assuming that Fe_3O_4 is the only magnetic responsive phase. Fig. 4d presents the room temperature magnetic hysteresis loops of the samples. Focusing on the saturation magnetization, a clear proportionality to the Fe_3O_4 percentage is observed. For instance, the sample with 25% Fe_3O_4 has a saturation magnetization value slightly over 20 emu/g, which reaches 60 emu/g for the sample with 75% Fe_3O_4 .

3.2. Adsorption efficiency

Batch adsorption experiments were performed to record the As(V) and Sb(V) isotherms for each of the tested nanocomposites and estimate the uptake capacity under water treatment conditions. Fig. 5 presents the adsorption isotherms for the $\text{Fe}_3\text{O}_4/\text{FeOOH}$ 50% nanocomposite. Due to the high affinity of FeOOH to As(V) species, the removal of arsenic appears much more efficient compared to that of Sb(V). As widely reported, the adsorption of $\text{HAsO}_4^{2-}/\text{H}_2\text{AsO}_4^-$ oxy-anions on FeOOH takes place through inner-sphere complexes appearing in bidentate mononuclear or binuclear configurations (Pinakidou et al., 2015; Sofia Tresintsi et al., 2013). On the other side, although inner-sphere chemisorption of antimony oxy-ions is possible, the high mobility of Sb(V) species and the ease of Sb(III) oxidation and re-dissolution prevent non-reversible adsorption (Qi and Pichler, 2016). However, the presence of a reducing agent such as Fe_3O_4 , features the material with the ability to capture non-negligible amounts of Sb(V) considering the poor response of previously tested adsorbents. The suggested intermediate reduction mechanism and the sole presence of Sb(III) on the nanocompos-

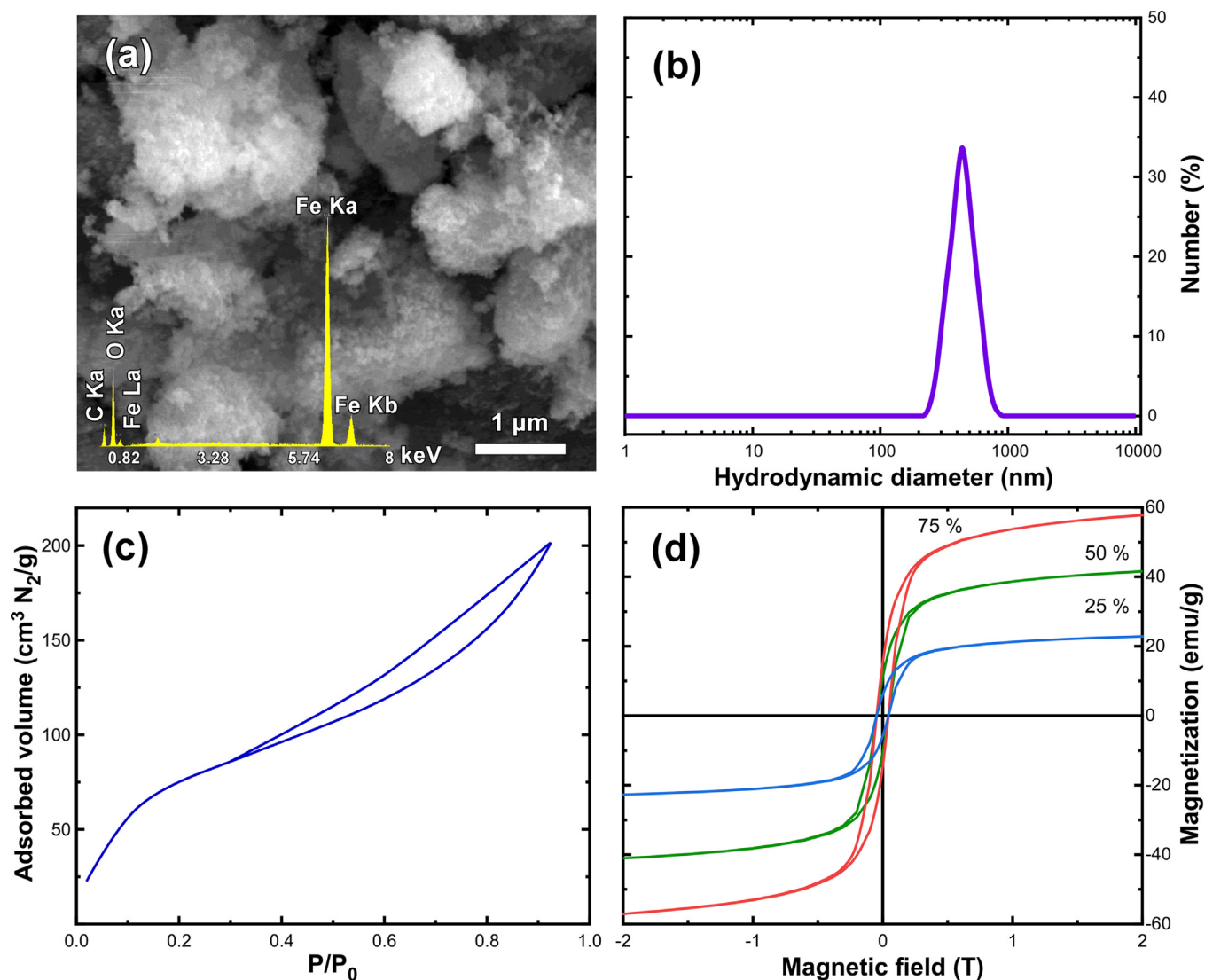


Fig. 4. FE-SEM image and EDS elemental analysis of Fe₃O₄/FeOOH 50% nanocomposite (a), hydrodynamic diameter numerical distribution (b) and gas nitrogen adsorption-desorption curve (c). Magnetic hysteresis loops of the studied samples for various magnetic phase percentages (d).

ite after experiment was validated by X-ray photoelectron spectroscopy as shown in Fig. S5 of Supporting information. In long terms, the participation of Fe₃O₄ as electron donor is expected to cause the passivation of its surface after the gradual formation of a maghemite's layer (Pinakidou et al., 2016). Surface passivation determines the operational lifetime of the developed adsorbent and it is the main reason for the difficulty to apply a typical regeneration process on the Fe₃O₄/FeOOH nanocomposite after its saturation. Importantly, observed adsorption capacities from experiments with only one of the pollutants in the solution are mostly preserved in the case of As(V) and Sb(V) co-existence as the corresponding isotherms indicate. This implies to a limited competition and interference between As(V) and Sb(V) at the low concentration range studied in this work and typically met in polluted groundwater sources. On the other hand, the reported negative effect of arsenic presence is signified by a sudden drop in Sb(V) capacity only when residual concentrations overcome 400 μg/L, corresponding to initial concentrations above 1.5 mg/L. The competition for adsorption sites becomes more intense and dramatically affects Sb(V) uptake when adsorption experiments are carried out at higher concentrations (Fig. S2 in Supporting information). Therefore, results from testing pollutants separately can be used to predict the adsorbents' efficiency in their co-existence. Fitting of the isotherms was carried out by the Freundlich equation, $Q=K_F$

$C_e^{1/n}$, with C_e the residual concentration, K_F a constant proportional to the uptake capacity, and n a constant related to the uptake affinity. The fitting parameters are shown in Table S1 in Supporting information.

By placing the maximum contaminant level for each pollutant (10 μg/L for As(V) and 5 μg/L for Sb(V)) as a residual concentration value in the fitted Freundlich equations, it is possible to calculate the adsorption capacity corresponding to the efficient operational period of the nanocomposites in real applications. The variation of these values with the Fe₃O₄ percentage in the nanocomposite is summarized in Fig. 6. Adsorption capacity for As(V) decreases linearly till Fe₃O₄ content reaches 50% and then, it is stabilized around a value of 2 mg/g. At the same time, the capacity for Sb(V) follows a continuous increase starting from almost zero for the pure FeOOH to around 0.4 mg/g at percentages above 50% Fe₃O₄. Accordingly, an obvious option to keep a balanced and affordable adsorption efficiency for both pollutants would be the Fe₃O₄/FeOOH 50% nanocomposite.

The uptake rate of the pollutants and the required contact time to reach equilibrium are essential information to design the adsorption reactor and estimate the flow rate of the treated water. The kinetic data recorded for the 50% nanocomposite (Fig. 7), indicates that more than 95% of the removal capacity at the equilibrium is already achieved before 1 h.

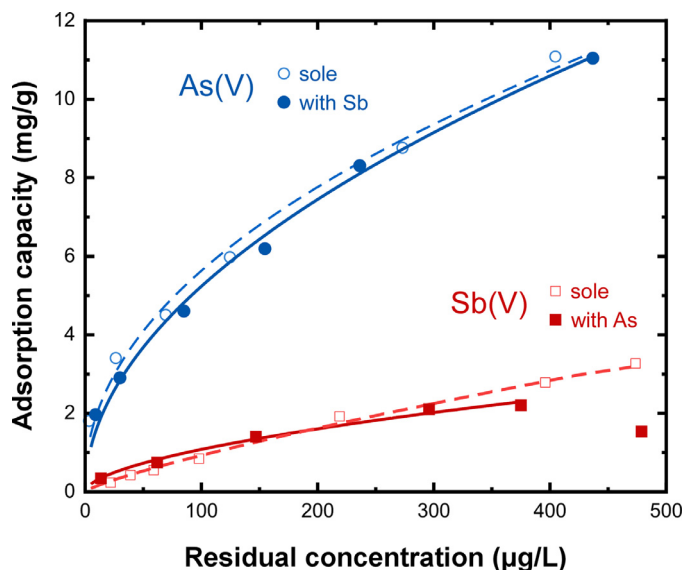


Fig. 5. Adsorption isotherms of As(V) and Sb(V) for the $\text{Fe}_3\text{O}_4/\text{FeOOH}$ 50% nanocomposite in natural-like water adjusted at pH 7. Fitting was performed by the Freundlich equation. Open circles and dotted lines indicate the corresponding specific isotherms of each pollutant when As(V) and Sb(V) are sole in the solution at equal initial concentrations.

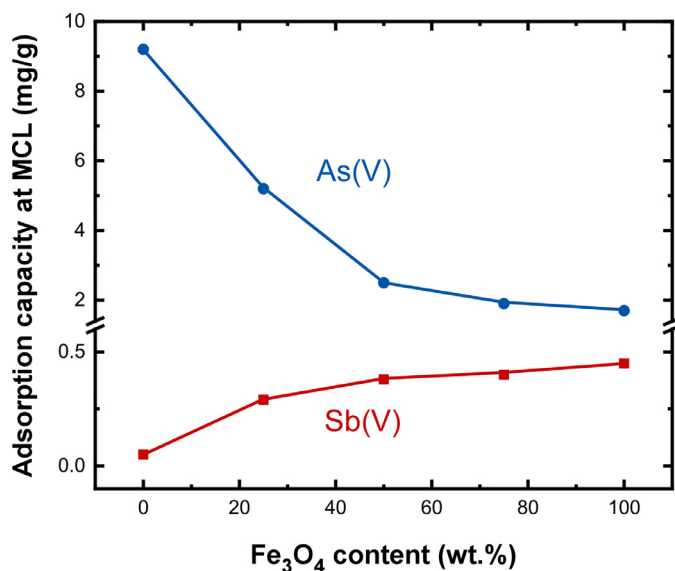


Fig. 6. Adsorption capacity at the maximum contaminant level of each pollutant (residual concentrations $10 \mu\text{g/L}$ for As, $5 \mu\text{g/L}$ for Sb) as a function of Fe_3O_4 percentage in the nanocomposite and pure phases. Values were estimated by adsorption isotherms carried out in natural-like water adjusted at pH 7.

3.3. Magnetic separation

The magnetic separator was modelled as an arrangement of eight cylindrical NdFeB magnets diametrically magnetized and positioned perpendicularly to the bottom side of the separation tube. To predict the optimal recovery efficiency of the magnetic separator, three magnetic fields induced by different polarity configurations were simulated and compared. At first, all magnets were arranged in order to have the same N/S orientation. On the second configuration, neighbor magnets were oppositely magnetized, while on the third, the polarity reversed among pairs of magnets, i.e. N/S for one pair and S/N for the other (Fig. S2).

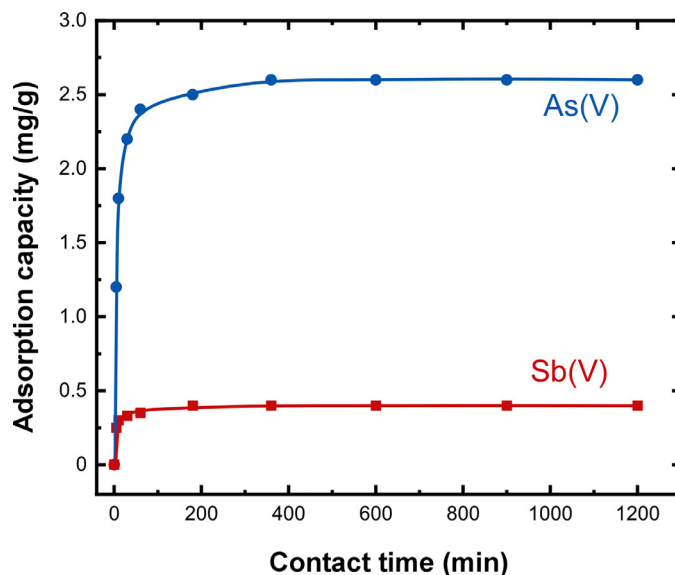


Fig. 7. Kinetic data of As(V) and Sb(V) removal for the $\text{Fe}_3\text{O}_4/\text{FeOOH}$ 50% nanocomposite in natural-like water adjusted at pH 7. Initial concentration As: $800 \mu\text{g/L}$, Sb: $150 \mu\text{g/L}$, adsorbent: 250 mg/L .

Besides pole configuration and magnetic phase, the effect of three more parameters was examined for each version of the separator, i.e. the tube radius R_t , the magnets' radius R_m and the distance d between magnets and tube. The tube radius varied from 0.25 cm to 1.0 cm, the magnets' radius from 0.5 cm to 2 cm, while the magnets-to-tube distance varied from 0.5 cm to 1 cm (Table 1). The distance between one magnet to another was considered equal to their corresponding radius in each case.

To measure the recovery efficiency of the magnetic separator, the motion of one hundred nanoparticles was simulated for every numeric combination of the parameters used in the theoretical model. For each setup, nanoparticles started from vertical positions, normally arranged along the tube's diameter, and their trajectories (Fig. S3) were computed by numerically solving the equations of motion with RK4 method. The ones that reached to the bottom side of the tube, above the magnets, were counted as successfully captured.

The percentages of estimated retrieved magnetic nanoparticles per case were compared among different configurations of the separator (Fig. 8), indicating the alternating polarity arrangement of magnets as the most efficient one. In tubes with radius larger than 0.25 cm, such a separator, consisting of large magnets ($R_m = 2 \text{ cm}$), eliminated more than 98% of the nanocomposites' 75% MPR sample and more than 80% of the 50% MPR sample, regardless the distance between magnets and tube. On the contrary, the highest yield was only 60% of the nanocomposites for the separator formed by similarly magnetized magnets. The separator with alternating polarity couples of magnets, recovered 45–93% of the 75% MPR nanoparticles, when its configuration involved large magnets ($R_m = 2 \text{ cm}$). Overall, out of the 144 combinations of model parameters per configuration, that were examined, those which led to significant elimination (more than 90%) of the magnetic nanoparticles sample were zero for the first configuration, 24 for the second and 2 for the third.

Results, also, imply that removal efficiency is proportional to both the diameters of tube and magnets, while their positions, i.e. tube's and magnets', needs to be as close as possible. Adequate clearance (more than 80%) of the particles was achieved in a few small separation tubes ($R_t = 0.25 \text{ cm}$). However, smaller magnets ($R_m = 0.5 \text{ cm}$) failed to remove particles under any one of the examined conditions. Total clearance of the sample mostly occurred where the separator was placed at minimum distance ($d = 0.5 \text{ cm}$) from the tube, as expected. Regarding the

Table 1
Parameters used in the theoretical model and their numeric values that were used to compute the trajectories of nanoparticles.

Property	Value	Property	Value
Permeability of free space (μ_0)	$4\pi \cdot 10^{-7}$ H/m	Particles' radius (R_p)	250 nm
Gravitational acceleration (g)	9.8 m/s ²	Magnetization of the magnets (M_s)	10^6 A/m
Fluid density (ρ_f)	1000 kg/m ³	Magnets' radius (R_m)	0.5, 1.0, 1.5, 2.0 cm
Water viscosity (η)	$8.9 \cdot 10^{-4}$ Pa s	Magnets-to-tube distance (d)	0.5, 0.75, 1.0 cm
Particles' density (ρ_p)	5000 kg/m ³	Volume flow rate (Q)	20 mL/min
Tube's radius (R_t)	0.25, 0.5, 0.75, 1.0 cm	Magnetic phase ratio (MPR)	25, 50, 75%

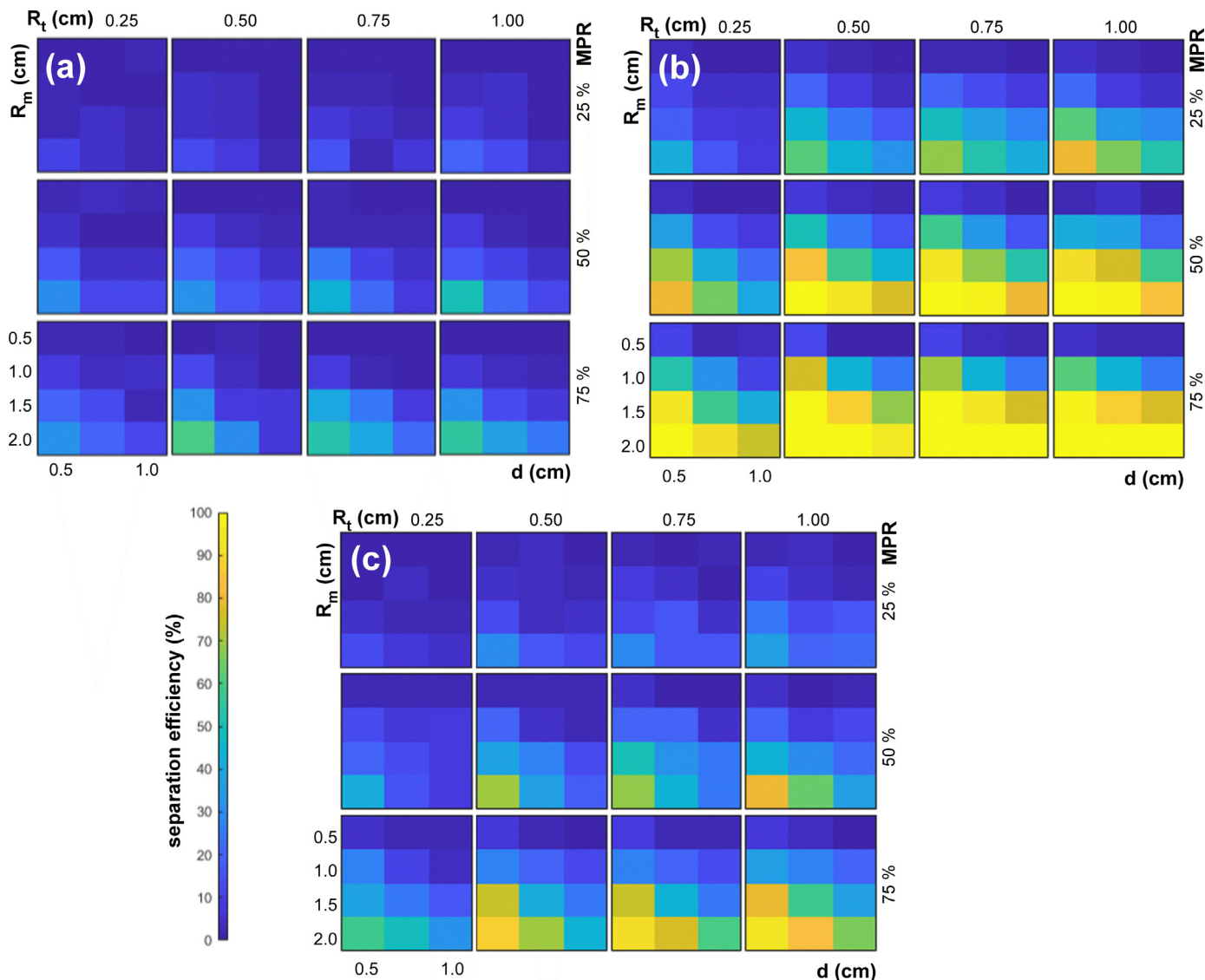


Fig. 8. Magnetic separator's efficiency per configuration: similar polarity magnets (a), alternating polarity magnets (b), alternating polarity couples of magnets (c). Color stands for retrieved nanoparticles percentage.

role of magnetic nanoparticles to the separation process, higher magnetic phase percentage in their composition ensures higher percentage of them ending captured by the magnetic field. Nanocomposites with 25% MPR failed to be successfully retrieved in almost all cases, with one exception of 80% clearance. On the other hand, several samples with 75% MPR were completely eliminated even by smaller magnets ($R_m=1.5$ cm) or distant separators ($d=1$ cm).

According to the results of the theoretical calculations and the kinetic data concerning pollutants adsorption, the laboratory continuous flow system was prepared using the following qualified construction and

operation parameters. A contact tank of 1.5 L was attached to the magnetic separator cylindrical tube with 0.5 m length and 0.75 cm diameter. A flow rate of 20 mL/min was applied to provide a contact time around 60 min which was found sufficient to allow achievement of adsorption equilibrium when the 50% nanocomposite was introduced. For the magnetic separator the alternating orientation of magnets with 2 cm in diameter was applied by placing the magnets at a distance 0.5 cm from the tube and between each other. Natural-like water adjusted at pH 7 spiked with 50 $\mu\text{g/L}$ As(V) and 10 $\mu\text{g/L}$ Sb(V) was used as a representative case of a polluted groundwater. The solid concentration was varied

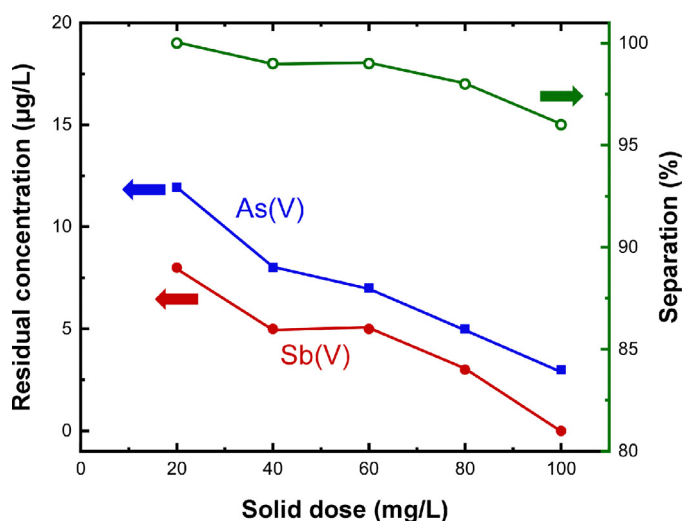


Fig. 9. Residual pollutants concentrations as a function of the nanocomposite dose in the contact reactor of the laboratory setup. The magnetic separation efficiency is also plotted.

in the range 20–100 mg/L. Fig. 9 summarizes the actual efficiency of the laboratory setup in view of the residual pollutants concentration and the percentage of captured nanocomposites in the outflow of the magnetic separator. For the lower dose of nanocomposite (20 mg/L), the residual As(V) and Sb(V) concentrations were determined slightly above the regulation limit for each one, a result that stands in good agreement with the estimated adsorption capacity from the corresponding isotherms. Increasing the dose improves efficiency of the process enabling residual concentrations not just within the regulation tolerance but approaching the detection limit for higher doses. Separation yield is 100% at lower solid concentration but remain at high levels till 100 mg/L.

4. Conclusions

The simultaneous capture of arsenic and antimony according to the requirements of drinking water use was succeeded by optimizing a multifunctional $\text{Fe}_3\text{O}_4/\text{FeOOH}$ nanocomposite able to provide a reducing agent (Fe_3O_4) for the Sb(V) conversion and a good adsorption substrate (FeOOH) for the capture of As(V) and the formed Sb(III). In spite of the chemical similarity between the two pollutants, the adsorption procedure seems to operate independently in the residual concentration range below 400 $\mu\text{g/L}$ suggesting the absence of competition of the uptake mechanisms or for the available sorption sites. In addition, the high magnetic response of Fe_3O_4 becomes advantageous towards the application of a water purification process based on simple contact combined with a magnetic separator. In the frame of this study, such possibility was validated by the design, based on theoretical calculations, and the operation of a continuous flow setup which enables the capture of toxic pollutants and the recovery of the used nanocomposite with minimum energy expense. Therefore, this work demonstrates how a complex problem of removing co-existing arsenic and antimony in a single step by a single adsorbent can be faced by the development of a binary nanocomposite and the sophisticated utilization of its magnetic response.

Declaration of Competing Interest

The authors declare that they have no known competing financial interests or personal relationships that could have appeared to influence the work reported in this paper.

CRedit authorship contribution statement

M. Tzirini: Methodology, Software, Writing - review & editing. **E. Kaprara:** Investigation. **T. Asimakidou:** Investigation, Data curation, Writing - original draft, Visualization. **K. Kontogiannopoulos:** Methodology, Data curation. **E. Tzamos:** Methodology, Data curation. **I. Kel-lartzis:** Data curation. **T. Samaras:** Methodology, Conceptualization, Writing - review & editing, Supervision. **Li Balcells:** Data curation, Validation. **M. Mitrakas:** Supervision. **K. Simeonidis:** Conceptualization, Writing - review & editing, Supervision.

Acknowledgments

This study was implemented within the frame of the action “Supporting Postdoctoral Researchers” of the Operational Program “Development of Human Resources, Education and Lifelong Learning 2014–2020” of IKY State Scholarships Foundation and is co-financed by the European Social Fund and the Greek State. Part of the measurements received funding from the EU-H2020 Research and Innovation Program under grant agreement No 654360 having benefitted from the access provided by CSIC-ICMAB in Barcelona within the framework of the NFFA-Europe Transnational Access Activity. Authors would like to thank Anna Esther Carrillo and Bernat Bozzo for the experimental assistance during SEM observations and SQUID measurements.

References

- Choong, T.S.Y., Chuah, T.G., Robiah, Y., Gregory Koay, F.L., Azni, I., 2007. Arsenic toxicity, health hazards and removal techniques from water: an overview. *Desalination* doi:10.1016/j.desal.2007.01.015.
- Chowdhury, S., Mazumder, M.A.J., Al-Attas, O., Husain, T., 2016. Heavy metals in drinking water: occurrences, implications, and future needs in developing countries. *Sci. Total Environ.* doi:10.1016/j.scitotenv.2016.06.166.
- Council Directive 98/83/EC, 2000. Council directive 98/83/EC of 3 November 1998 on the quality of water intended for human consumption. *Off. J. Eur. Communities* 2004R0726-v.7of05.06.2013.
- Fei, J.C., Min, X.B., Wang, Z.X., Pang, Z.hua, Liang, Y.J., Ke, Y., 2017. Health and ecological risk assessment of heavy metals pollution in an antimony mining region: a case study from South China. *Environ. Sci. Pollut. Res.* doi:10.1007/s11356-017-0310-x.
- Furlani, E.J., Furlani, E.P., 2007. A model for predicting magnetic targeting of multifunctional particles in the microvasculature. *J. Magn. Magn. Mater.* doi:10.1016/j.jmmm.2006.09.026.
- Furlani, E.P., Ng, K.C., 2006. Analytical model of magnetic nanoparticle transport and capture in the microvasculature. *Phys. Rev. E Stat. Nonlinear Soft Matter Phys.* doi:10.1103/PhysRevE.73.061919.
- Gannon, K., Wilson, D.J., 1986. Removal of antimony from aqueous systems. *Sep. Sci. Technol.* 21, 475–493. doi:10.1080/01496398608056130.
- Geissen, V., Mol, H., Klumpp, E., Umlauf, G., Nadal, M., van der Ploeg, M., van de Zee, S.E.A.T.M., Ritsema, C.J., 2015. Emerging pollutants in the environment: a challenge for water resource management. *Int. Soil Water Conserv. Res.* doi:10.1016/j.iswcr.2015.03.002.
- Hu, G., Bakhtavar, E., Hewage, K., Mohseni, M., Sadiq, R., 2019. Heavy metals risk assessment in drinking water: an integrated probabilistic-fuzzy approach. *J. Environ. Manag.* doi:10.1016/j.jenvman.2019.109514.
- Joint Center for Powder Diffraction Studies, 2004. *Powder Diffraction File. International Centre for Diffraction Data, Newtown Square, PA.*
- Kaltreider, R.C., Davis, A.M., Lariviere, J.P., Hamilton, J.W., 2001. Arsenic alters the function of the glucocorticoid receptor as a transcription factor. *Environ. Health Perspect.* doi:10.1289/ehp.01109245.
- Karavoltos, S., Sakellari, A., Mihopoulos, N., Dassenakis, M., Scoullou, M.J., 2008. Evaluation of the quality of drinking water in regions of Greece. *Desalination* doi:10.1016/j.desal.2007.06.013.
- Lakshmanan, D., Clifford, D.A., Samanta, G., 2010. Comparative study of arsenic removal by iron using electrocoagulation and chemical coagulation. *Water Res.* doi:10.1016/j.watres.2010.06.018.
- Mitrakas, M.G., Panteliadis, P.C., Keramidis, V.Z., Tzimou-Tsitouridou, R.D., Sikalidis, C.a., 2009. Predicting Fe^{3+} dose for As(V) removal at pHs and temperatures commonly encountered in natural waters. *Chem. Eng. J.* 155, 716–721. doi:10.1016/j.cej.2009.09.011.
- Mohan, D., Pittman, C.U., 2007. Arsenic removal from water/wastewater using adsorbents: a critical review. *J. Hazard. Mater.* doi:10.1016/j.jhazmat.2007.01.006.
- Nicemel, N.R., Leus, K., Folens, K., Van Der Voort, P., Du Laing, G., 2015. Technologies for arsenic removal from water: current status and future perspectives. *Int. J. Environ. Res. Public Health* doi:10.3390/ijerph13010062.
- Pinakidou, F., Katsikini, M., Simeonidis, K., Kaprara, E., Paloura, E.C., Mitrakas, M., 2016. On the passivation mechanism of Fe_3O_4 nanoparticles during Cr(VI) removal from water: a XAFS study. *Appl. Surf. Sci.* 360, 1080–1086. doi:10.1016/j.apsusc.2015.11.063.

- Pinakidou, F., Katsikini, M., Simeonidis, K., Paloura, E.C., Mitrakas, M., 2015. An X-ray absorption study of synthesis- and As adsorption-induced microstructural modifications in Fe oxy-hydroxides. *J. Hazard. Mater.* 298, 203–209. doi:10.1016/j.jhazmat.2015.05.037.
- Qi, P., Pichler, T., 2016. Sequential and simultaneous adsorption of Sb(III) and Sb(V) on ferrihydrite: implications for oxidation and competition. *Chemosphere* 145, 55–60. doi:10.1016/j.chemosphere.2015.11.057.
- Sankar, M.U., Aigal, S., Maliyekkal, S.M., Chaudhary, A., Anshup, Kumar, A.A., Chaudhari, K., Pradeep, T., 2013. Biopolymer-reinforced synthetic granular nanocomposites for affordable point-of-use water purification. *Proc. Natl. Acad. Sci. U. S. A.* 110, 8459–8464. doi:10.1073/pnas.1220222110.
- Sarkar, A., Paul, B., 2016. The global menace of arsenic and its conventional remediation - a critical review. *Chemosphere* doi:10.1016/j.chemosphere.2016.05.043.
- Scheinost, A.C., Rossberg, A., Vantelon, D., Xifra, I., Kretzschmar, R., Leuz, A.K., Funke, H., Johnson, C.A., 2006. Quantitative antimony speciation in shooting-range soils by EXAFS spectroscopy. *Geochim. Cosmochim. Acta* 70, 3299–3312. doi:10.1016/j.gca.2006.03.020.
- Schwarzenbach, R.P., Egli, T., Hofstetter, T.B., von Gunten, U., Wehrli, B., 2010. Global water pollution and human health. *Annu. Rev. Environ. Resour.* doi:10.1146/annurev-environ-100809-125342.
- Sharma, S., Katiyar, V.K., Singh, U., 2015. Mathematical modelling for trajectories of magnetic nanoparticles in a blood vessel under magnetic field. *J. Magn. Magn. Mater.* doi:10.1016/j.jmmm.2014.12.012.
- Simeonidis, K., Gkinis, T., Tresintsi, S., Martinez-Boubeta, C., Vourlias, G., Tsiaousis, I., Stavropoulos, G., Mitrakas, M., Angelakeris, M., 2011. Magnetic separation of hematite-coated Fe₃O₄ particles used as arsenic adsorbents. *Chem. Eng. J.* 168, 1008–1015. doi:10.1016/j.cej.2011.01.074.
- Simeonidis, K., Kalaitzidou, K., Kaprara, E., Mitraka, G., Asimakidou, T., Balcells, L., Mitrakas, M., 2019. Uptake of Sb(V) by nano Fe₃O₄-decorated iron oxy-hydroxides. *Water* 11. doi:10.3390/w11010181.
- Simeonidis, K., Kaprara, E., Samaras, T., Angelakeris, M., Pliatsikas, N., Vourlias, G., Mitrakas, M., Andritsos, N., 2015. Optimizing magnetic nanoparticles for drinking water technology: the case of Cr(VI). *Sci. Total Environ.* 535, 61–68. doi:10.1016/j.scitotenv.2015.04.033.
- Tresintsi, Sofia, Simeonidis, K., Estradé, S., Martinez-Boubeta, C., Vourlias, G., Pinakidou, F., Katsikini, M., Paloura, E.C., Stavropoulos, G., Mitrakas, M., 2013. Tetravalent manganese ferrihydrite: a novel nanoadsorbent equally selective for As(III) and As(V) removal from drinking water. *Environ. Sci. Technol.* 47, 9699–9705. doi:10.1021/es4009932.
- Tresintsi, S., Simeonidis, K., Vourlias, G., Stavropoulos, G., Mitrakas, M., 2012. Kilogram-scale synthesis of iron oxy-hydroxides with improved arsenic removal capacity: study of Fe(II) oxidation-precipitation parameters. *Water Res.* 46, 5255–5267. doi:10.1016/j.watres.2012.06.049.
- Tresintsi, S., Simeonidis, K., Zouboulis, A., Mitrakas, M., 2013. Comparative study of As(V) removal by ferric coagulation and oxy-hydroxides adsorption: laboratory and full-scale case studies. *Desalin. Water Treat.* 51, 2872–2880. doi:10.1080/19443994.2012.748011.
- Ungureanu, G., Santos, S., Boaventura, R., Botelho, C., 2015. Arsenic and antimony in water and wastewater: overview of removal techniques with special reference to latest advances in adsorption. *J. Environ. Manag.* doi:10.1016/j.jenvman.2014.12.051.
- Wells, M.J.M., Bell, K.Y., Traexler, K.A., Pellegrin, M.-L., Morse, A., 2010. Emerging pollutants. *Water Environ. Res.* doi:10.2175/106143010x1275666880292.